REPORT DOCUMENTATION PAGE

Form Approved
OMB No. 0704-0188

1. AGENCY USE ONLY (Leave Blank)	2. REPORT DATE	3. REPORT TYPE AND DATES COVERED
	July 1, 2005	Final Report June 28, 2002 - June 28, 2005

4. TITLE AND SUBTITLE
"Advanced MHD Alogoritihm for Solar and Space Science"

5. FUNDING NUMBERS
NAS5-02085

6. AUTHORS
Dalton D. Schnack

7. PERFORMING ORGANIZATION NAME(S) AND ADDRESS(ES)

Science Applications International Corporation
10260 Campus Point Drive, MS H4A
San Diego, CA 92121-1578 (Email: lionellor@saic.com)

8. PERFORMAING ORGANIZATION REPORT NUMBER
SAIC-04/8007
01-1339-04-4478-100

9. SPONSORING/MONITORING AGENCY NAME(S) AND ADDRESS(ES)

NASA Headquarters
Goddard Space Flight Center
Greenbelt, MD 20771

10. SPONSORING/MONITORING AGENCY REPORT NUMBER

11. SUPPLEMENTARY NOTES

12a. DISTRIBUTION/AVAILABILITY STATEMENT
X Approved for public release; distribution unlimited.
Distribution limited to U. S. Government agencies only - report contains proprietary information.

12b. DISTRIBUTION CODE

13. ABSTRACT *(Maximum 200 words)*
We report progress in the development of MH4D (MHD code on a tetrahedral domain) during the three years of performance. We discuss the implementation of new features in the algorithm, validations of the computational model, presentations at several conferences, and the overcoming of issues that occurred during code development.

14. SUBJECT TERMS
Solar Wind, Coronal Magnetic Field, Magnetohydrodynamics

15. NUMBER OF PAGES
37

16. PRICE CODE

17. SECURITY CLASSIFICATION OF REPORT	18. SECURITY CLASSIFICATION OF THIS PAGE	19. SECURITY CLASSIFICATION OF ABSTRACT	20. LIMITATION OF ABSTRACT
UNCLASSIFIED	UNCLASSIFIED	UNCLASSIFIED	ULIMITED

Advance MHD Algorithm for Solar and Space Science
Final Report

June 28, 2002 – June 28, 2005

We report progress for the development of MH4D during the three years of performance. The following features have been implemented into the code:

- Implementation of centered and upwinded operators
- Implementation of the Hydrodynamic equations
- Implementation of the MHD equations.
- Implementation of the semi-implicit algorithm.
- Development of a cell-centered advection scheme for the momentum equation.
- Propagation of a disturbance in the supersonic solar wind.

The following presentations were given at these meetings:

- Presentation of a poster at 2002 Fall AGU Meeting, 6-10 December 2002, San Francisco, CA.
- Presentation of a poster at the EGS-AGU-EUG Joint Assembly in Nice, France, April 6-11, 2003.
- Presentation of a poster at the 2003 International Sherwood Theory Conference in Corpus Christi, Texas, April 28-30 2003.
- Presentation of a poster at the AGU Fall Meeting in San Francisco, California, December 8-12, 2003.
- Presentation of a poster at the 2004 Joint Assembly (CGU, AGU, SEG, and EEGS) in Montreal, Canada, May 17-21, 2004.
- Presentation of a poster at the 2004 Fall AGU Meeting to be held in San Francisco, CA, December 13-17, 2004.
- Oral Presentation at the 2005 AISRP PI Meeting that was held at the NASA Ames Research Center, on April 4-6, 2005
- Presentation of a poster at the 2005 Joint Assembly that was held in New Orleans, LA, on May 23-27, 2005.

Validation of the new features implemented in the code and modeling:

- The Sod's problem.
- Alfvén waves in a cylinder.

- The nonlinear kink mode in the unstable Gold-Hoyle equilibrium.
- The MHD shock problem (Brio, M. and Wu, C. C., J. Comp. Phys. 75, 400 , 1988)
- Supersonic solar wind problem
- Propagation of a disturbance in the supersonic solar wind.

In the following sections we present details broken down by period of performance.

MH4D Progress Report

3rd and 4th Quarters FY03

June 28, 2002 – December 28, 2002

We report progress for the development of MH4D for the third and fourth quarters of FY2003, June 28 – December 28, 2002. The present version of MH4D can now

- Solve the implicit, resistive diffusion equation for a given tangential vector potential specified at the boundaries.
- Solve the explicit, viscous, nonlinear hydrodynamic equations.

In this report we describe progress in the following areas

- *Presentation of a Poster at 2002 Fall AGU Meeting.*
- *Code Development.*
  - Implementation of Centered and Upwinded Operators
  - Implementation of the Hydrodynamic Equations
- *Validation of the New Features Implemented in the Code.*

Details are given in the following sections.

1. PRESENTATION OF A POSTER AT 2002 FALL AGU MEETING

We have attended the 2002 Fall American Geophysical Union Meeting that was held in San Francisco, CA between 5 and 10 December 2002. A poster illustrating the structure of the code and the most recent result was presented. (R. Lionello and Dalton D. Schnack ``MH4D, an MHD Algorithm on an Unstructured Tetrahedral Grid'', *Eos Trans. AGU, 83*(47), Fall Meet. Suppl., Abstract SH52A-0492, 2002). The text of the abstract follows:

> We report our progress in the development of MH4D (Magnetohydrodynamics on a TETRAhedral Domain). MH4D is a massively-parallel, device-independent numerical code for the solution of the resistive and viscous MHD equations on an unstructured grid of tetrahedra. The unstructured mesh allows the resolution to be increased in the regions of physical interest. Consequently, MH4D can model problems with a wide range of spatial scales (e.g., active regions in the large scale corona). A variational formulation of the differential operators ensures accuracy and the preservation of the analytical properties of the operators ($\nabla \cdot \mathbf{B} = 0$)and elf-adjointness of the resistive and viscous operators. The combined semi-implicit treatment of the waves and implicit formulation of the diffusive operators can accommodate the wide ange of time scales present in the solar corona. The capability of mesh refinement and coarsening is also included. MH4D is currently capable of solving the resistive diffusion equation and he equations of hydrodynamics. Preliminary results will be presented.

2. CODE DEVELOPMENT

2.1 Implementation of Centered and Upwinded Operators

We have implemented subroutines to calculate the gradient and divergence of vertex or centroid based fields on the mesh exemplified in Fig. 1a. Centroids are indicated in capital letters and vertices in lower case letters. In MH4D the divergence of vector field $\mathbf{v}_i$ defined on vertices is calculated on centroids according to

$$(\nabla \cdot \mathbf{v})_I = \frac{1}{V_I} \sum_i \mathbf{S}_I \cdot \bar{\mathbf{v}}_i, \tag{1}$$

where, the sum is over the faces surrounding tetrahedron I, V_I is the tetrahedron volume, $\mathbf{S}_i$ is the vector area of the face opposite to vertex i, and we use an overscore to indicate the average value of $\mathbf{v}$ on face $\mathbf{S}_i$ (see Fig. 1b).

The gradient of a scalar field p_I defined on centroids is calculated on vertices as follows

$$(\nabla p)_i = \frac{1}{V_i} \sum_I \mathbf{s}_I p_I, \tag{2}$$

where V_i is the volume surrounding vertex i, the sum is over the dual faces surrounding i, $\mathbf{s}_I$ is the vector area shown in red in Fig. 1c. We have also implemented operators for scalar quantities on vertices and vector quantities on centroids.

When advecting a scalar or vector field, the divergence is calculated in an upwinded way. For example when advecting a scalar quantity with a velocity field $\mathbf{v}$, the governing equation

$$\frac{\partial \rho}{\partial t} = -\nabla \cdot \rho \mathbf{v} \tag{3}$$

can be implemented numerically according to the following formula

$$\frac{\Delta \rho_I}{\Delta t} = -\frac{1}{V_I} \sum_i \mathbf{S}_i^I \cdot \bar{\mathbf{v}}_i \rho_{U(i)}, \tag{4}$$

$$\rho_{U(i)} = \begin{cases} \rho_I & \text{if } \mathbf{S}_i^I \cdot \bar{v}_i \geq 0 \\ \rho J & \text{if } \mathbf{S}_i^I \cdot \bar{v}_i < 0 \end{cases}. \tag{5}$$

Hence the value of $\rho_{U(i)}$ is chosen according to the sign of the flux at the face shared between tetrahedra I and J (Fig. 1b).

When advecting a vector quantity $\mathbf{p}$ according to

$$\frac{\partial \mathbf{p}}{\partial t} = -\nabla \cdot \mathbf{p}\mathbf{v}, \tag{6}$$

the numerical implementation is

$$\frac{\Delta \mathbf{p}_i}{\Delta t} = -\frac{1}{Vi} \sum_E \mathbf{S}_i^E \cdot \bar{\mathbf{v}}^{-E} \mathbf{p}_{u(E)}, \tag{7}$$

$$\rho_{U(i)} = \begin{cases} \rho_I & \text{if } \mathbf{S}_i^I \cdot \bar{v}_i \geq 0 \\ \rho J & \text{if } \mathbf{S}_i^I \cdot \bar{v}_i < 0 \end{cases}. \tag{8}$$

$\bar{\mathbf{v}}^{E}$ is the velocity averaged at the edge connecting two vertices and $\mathbf{S}_i^E$ is the vector area associated with the edge (Fig. 1d).

2.2 Implementation of the Hydrodynamic Equations

The gradient and divergence operators, whose implementation is described in the previous section, are now used in MH4D to advance the viscous hydrodynamic equations:

$$\frac{\partial \rho}{\partial t} + \nabla \cdot (\rho \mathbf{v}) = 0 \tag{9}$$

$$\frac{\partial p}{\partial t} + \nabla \cdot (p\mathbf{v}) = -(\gamma - 1) p \nabla \cdot \mathbf{v} \tag{10}$$

$$\rho\left(\frac{\partial \mathbf{v}}{\partial t} + \mathbf{v} \cdot \nabla \mathbf{v}\right) = -\nabla p + \nabla \cdot (\nu \rho \nabla \mathbf{v}) \tag{11}$$

ρ and p are the plasma density and pressure, γ is the specific heat ratio, $\mathbf{v}$ is the velocity, and ν is the viscosity. The viscosity operator is implemented by applying first a gradient and then a divergence operator in order. Time advancement is currently an explicit leap-frog scheme for the wave operators and first order upwinding for advection.

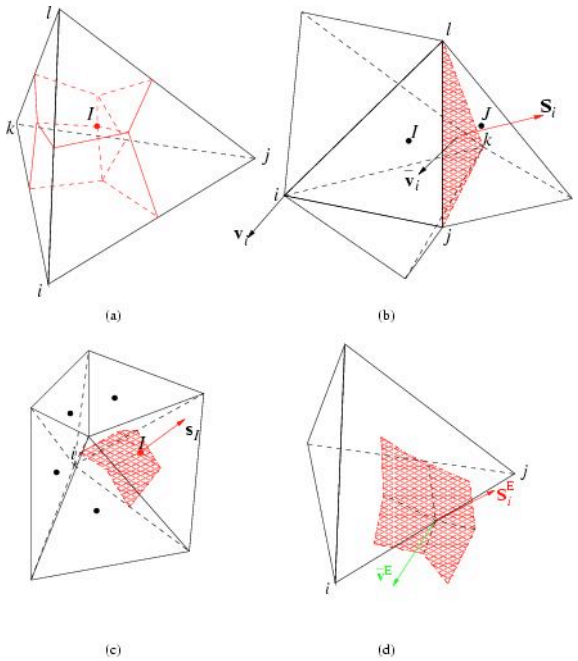

FIG. 1. Mesh elements, faces, and edges. Mesh and dual mesh edges; dual mesh edges are in red; the cell centroid indicated with a dot (a). Divergence operator applied on v, a vertex centered field (b). Gradient operator applied on a cell centered field (c). Advection of vertex based vector field (d).

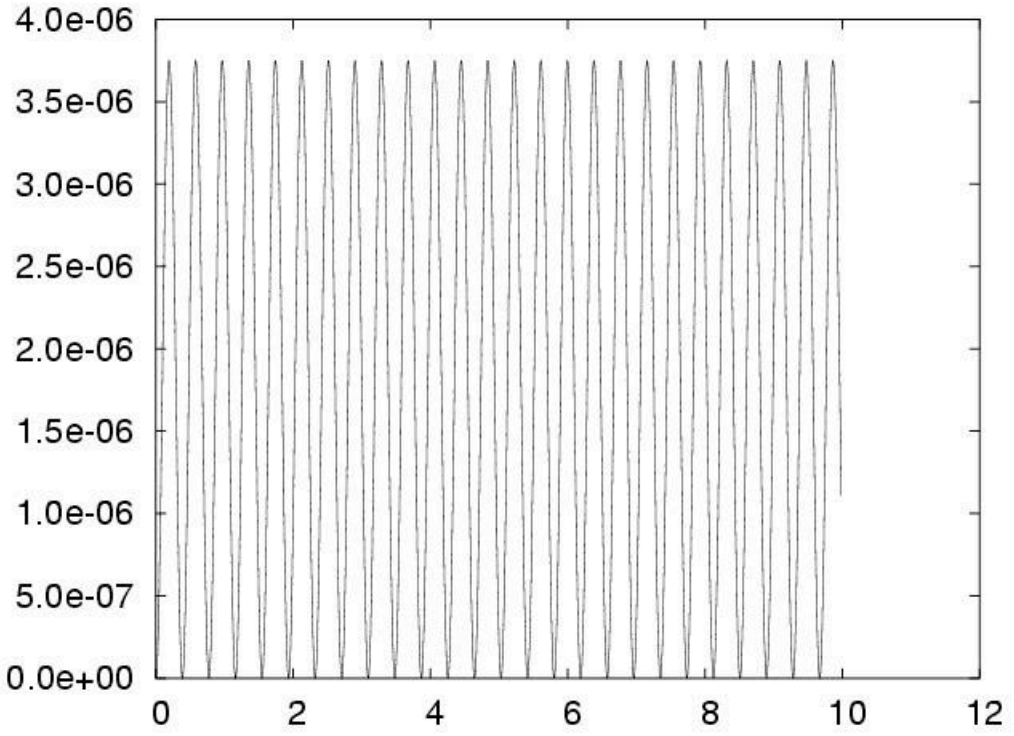

FIG. 2. Kinetic energy as a function of time for the case of the sound wave eigenmode in a box.

3. VALIDATION OF THE NEW FEATURES IMPLEMENTED IN THE CODE

We have tested the implementation of the hydrodynamic algorithm by reproducing eigenfunctions of the linearized fluid equations (i.e. sound waves). The equations for linear sound waves are

$$\frac{\partial \rho}{\partial t} + \nabla \cdot (\rho \mathbf{v}) = 0, \tag{12}$$

$$\frac{\partial p}{\partial t} + \nabla \cdot (p \mathbf{v}) = -(\gamma - 1) p \nabla \cdot \mathbf{v}. \tag{13}$$

We have used δ to indicate the perturbed quantities. A solution (eigenvector) in a box is

$$\begin{cases} \delta v_x = \varepsilon \sin \omega t \sin kx \\ \delta p = \varepsilon \sqrt{\gamma p \rho} \cos \omega t \cos kx \end{cases}, \tag{14}$$

with angular speed

$$\omega = k \sqrt{\frac{\gamma p}{\rho}} \tag{15}$$

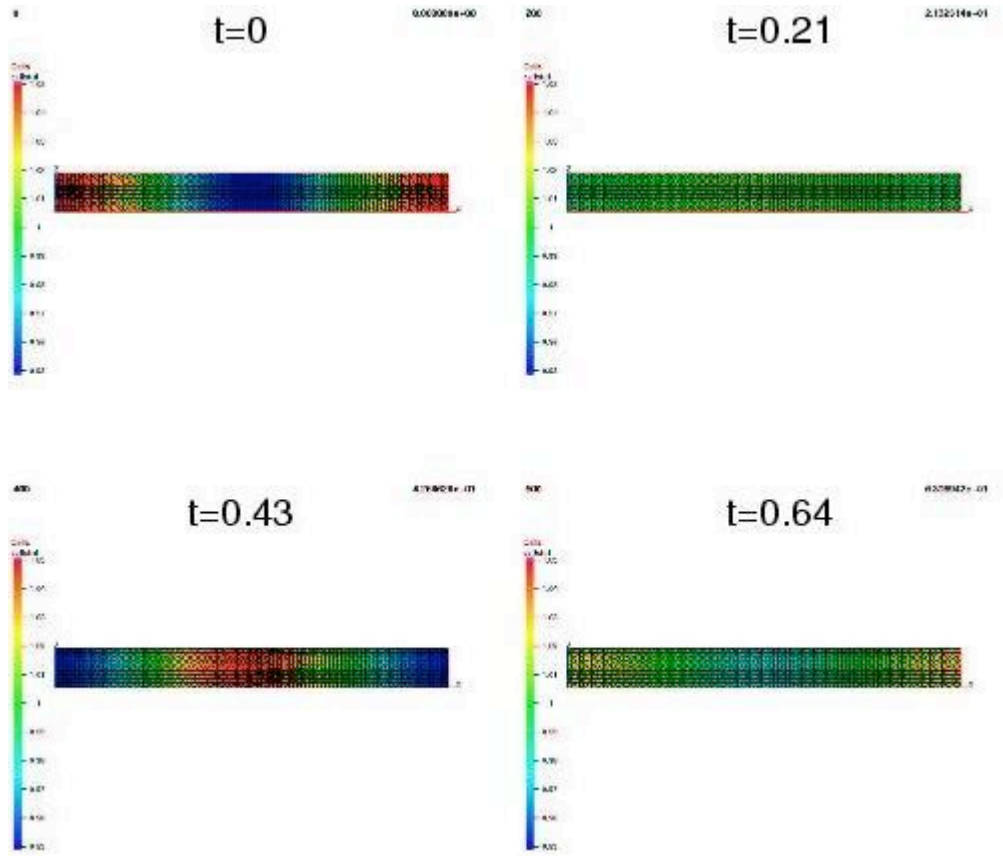

FIG. 3. The mesh colored according to the pressure perturbation at four instants in time for the case of the sound wave eigenmode in a box.

For $k = 2\pi$, $\rho = 1$, $\gamma = 5/3$, $p = 1$, the theoretical period is $T = 0.77450$. We have designed a grid of 10000 vertices and 47623 cells. The dimensions of the grid are 1 _ 0.1 _ 0.1. We have applied the perturbation as in Eq. (14) and advanced Eqs. (9-11) with MH4D. The period calculated by MH4D is $T_c = 0.7750$. Figure 2 shows the kinetic energy whose period is one half. Figure 3 has four panels representing the mesh at four instants in time during one period. The edges of the mesh are shown and the cells are colored according to the value of the pressure perturbation.

An eigenmode of the sound wave equation in a sphere is

$$\begin{cases} \delta v_r = \varepsilon \sin \omega t \left(\dfrac{\cos kr}{kr} - \dfrac{\sin kr}{(kr)^2} \right), \\ \delta p = \varepsilon \sqrt{\gamma p \rho} \cos \omega t \dfrac{\sin kr}{kr} \end{cases} \tag{16}$$

with angular speed

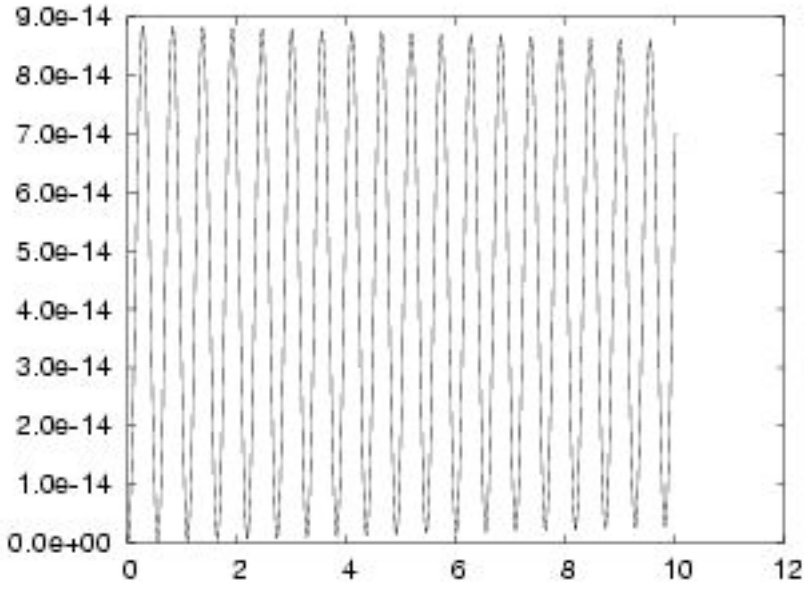

FIG. 4. Kinetic energy as a function of time for the case of the sound wave eigenmode. in a sphere.

(17) $$\omega = k\sqrt{\frac{\gamma p}{\rho}}$$

for $k = 4.493409$, $\rho = 1$, $\gamma = 5/3$, $p = 1$, the theoretical period is $T = 1.0831$. A spherical mesh of 12541 vertices and 66560 cells has been used for the calculation with MH4D. The radius of the sphere is 1. The calculated period is $T_c = 1.0867$. Figure 4 shows the kinetic energy during the simulation and Fig. 5 shows a cut of the mesh passing through the center of the sphere. The cells are colored according to the value of the pressure perturbation.

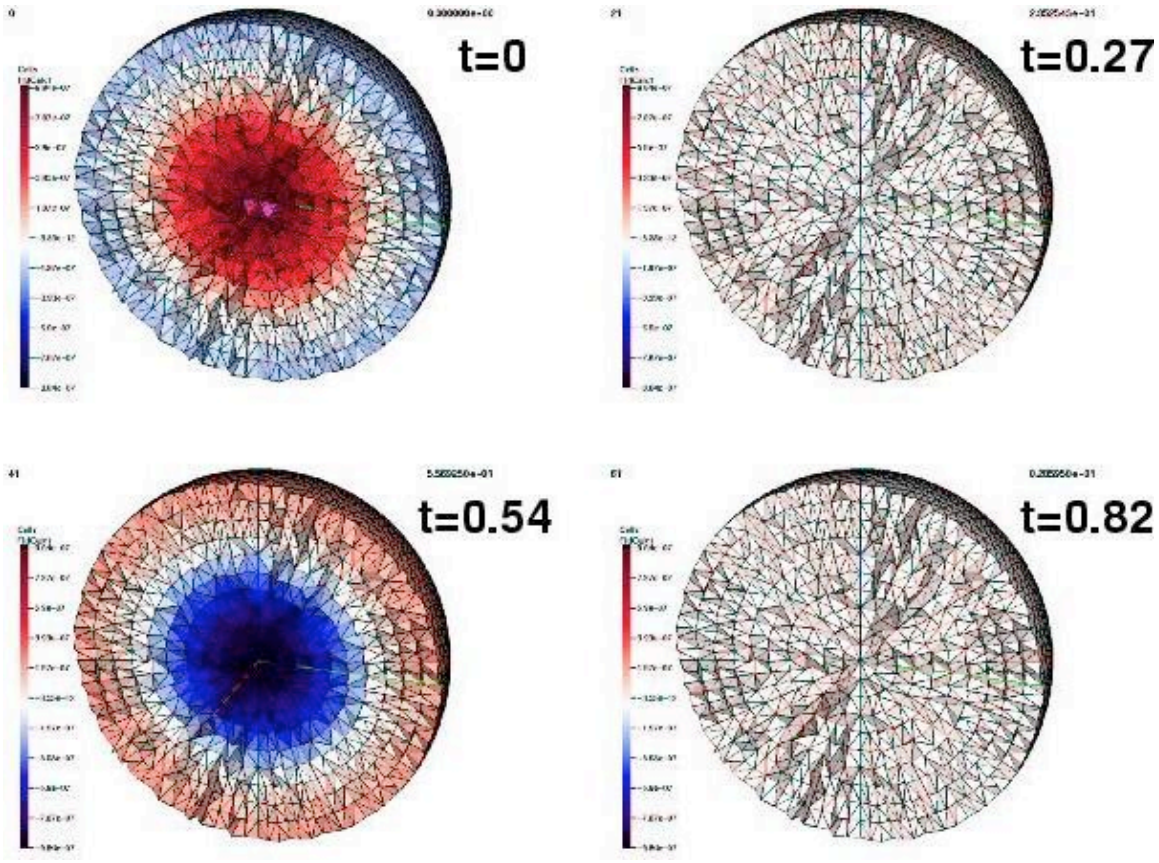

FIG. 5. A cut of the spherical mesh showing the pressure perturbation at four instants in time for the case of the sound wave eigenmode in a sphere.

MH4D Progress Report

1st and 2nd Quarters FY04

December 29, 2002 – June 6, 2003

We report progress for the development of MH4D for the first and second quarters of FY2004, December 29, 2002 – June 6, 2003. The present version of MH4D can now solve the *full viscous and resistive MHD equations* using either an explicit or a semi-implicit time advancement algorithm. This fulfills with what we promised in the proposal.

In this report we describe progress in the following areas

- *Presentation of a Poster at the EGS-AGU-EUG Joint Assembly in Nice, France, April 6-11, 2003.*
- *Presentation of a Poster at the 2003 International Sherwood Theory Conference in Corpus Christi, Texas, April 28-30 2003.*
- *Code Development.*
  - Implementation of the MHD equations.
  - Implementation of the semi-implicit algorithm.
- *Validation of the New Features Implemented in the Code*
  - The Sod's problem.
  - Alfvén waves in a cylinder.

Details are given in the following sections.

1. PRESENTATION OF A POSTER AT EGS-AGU-EUG JOINT ASSEMBLY

We have attended the EGS-AGU-EUG Joint Assembly that was held in Nice, France between 6 and 11 April 2003. A poster illustrating the structure of the code and the most recent result was presented. (Dalton D. Schnack and Roberto Lionello `` Developing an MHD Algorithm on an Unstructured Mesh of Tetrahedra'', *Geophysical Research Abstracts, Vol. 5, 04691, 2003*). The text of the abstract follows:

> MH4D (Magnetohydrodynamics on a TETRAhedral Domain) is a massively-parallel, device-independent numerical code for the solution of the resistive and viscous MHD equations on an unstructured grid of tetrahedra. The unstructured grid allows the resolution to be increased in the regions of physical interest. Consequently, MH4D can model problems with a wide range of spatial scales (e.g., active regions in the large scale corona). A variational formulation of the differential operators ensures accuracy and the preservation of the analytical properties of the operators ($\nabla \cdot \mathbf{B} = 0$) and self-adjointness of the resistive and viscous operators. The combined semi-implicit treatment of the waves and implicit formulation of the diffusive operators can accommodate the wide range of time scales present in the

solar corona. The capability of mesh refinement and coarsening is also included. MH4D is currently capable of solving the resistive diffusion equation and the equations of hydrodynamics. We will present preliminary results.

2. PRESENTATION OF A POSTER AT THE SHERWOOD CONFERENCE

We have attended the 2003 International Sherwood Theory Conference that was held in Corpus Christi between 28 and 30 April 2003. A poster illustrating the structure of the code and the most recent result was presented. (R. Lionello and D. D. Schnack `` MH4D: an MHD Algorithm on an Unstructured Tetrahedral Grid'', *1E37*). The text of the abstract follows:

> MH4D (Magnetohydrodynamics on a TETRAhedral Domain) is a massively-parallel, device-independent numerical code for the solution of the resistive and viscous MHD equations on an unstructured grid of tetrahedra. The unstructured grid allows the resolution to be increased in the regions of physical interest. Consequently, MH4D can model problems with a wide range of spatial scales (e.g., active regions in the large scale corona). A variational formulation of the differential operators ensures accuracy and the preservation of the analytical properties of the operators ($\nabla \cdot \mathbf{B} = 0$), and self-adjointness of the resistive and viscous operators. The combined semi-implicit treatment of the waves and implicit formulation of the diffusive operators can accommodate the wide range of time scales present in the solar corona. The capability of mesh refinement and coarsening is also included. MH4D is currently capable of solving the resistive diffusion equation and the equations of hydrodynamics. We are currently implementing the MHD operators and will present preliminary results.

3. CODE DEVELOPMENT

MH4D can now solve the full resistive and viscous MHD equations:

(1) $$\mathbf{B} = \nabla \times \mathbf{A}$$

(2)

(3) ——

(4) $$\frac{\partial \rho}{\partial t} + \nabla \cdot (\rho \mathbf{v}) = 0$$

(5) $$\frac{\partial p}{\partial t} + \nabla \cdot (p\mathbf{v}) = -(\gamma - 1) p \nabla \cdot \mathbf{v}$$

(6) ——

This set of equations can be advanced explicitly or semi-implicitly. We describe now how the magnetic operators and the semi-implicit solve have been implemented.

3.1 Implementation of the MHD Equations.

We have implemented subroutines to calculate the advective term in the induction equation for the vector potential and the Lorentz's force term in the momentum equation. The advection term, calculated on vertex *i*, has been written as

(7) $$(\mathbf{v}\times\overline{\mathbf{B}})_i = \mathbf{v}_i \times \frac{1}{N_i}\sum_{I(i)=1}^{N_i}\mathbf{B}_{I(i)},$$

where the value of the magnetic field, , is the average of all the values of the magnetic field located on the centroids surrounding vertex *i.*

The expression for the Lorentz's force term is

(8) — ——

is the volume of the centroid *I* surrounding vertex *i* and V_i is the volume of the dual mesh element centered on vertex *i*. This volume average has been introduced to preserve the self-adjointness of the numerical representation of the MHD operator.

3.1 Implementation of the Semi-Implicit Algorithm

In the lower corona, the Alfvén and sound speed are large compared with the speed of the flow. An explicit algorithm would require a very small time-step to follow the propagation of short-wavelength, high frequency waves that are of minimal importance for the dynamics of the systems we want to model. For this reason we apply a semi-implicit treatment to the wave-like terms. A semi-implicit formulation avoids the time-step restriction imposed by high frequency compressional and torsional Alfvén waves and allows for an arbitrarily large time-step with respect to the normal modes of the system.. In order to implement the semi-implicit method, the momentum equation has been modified as follows:

(9) — —,

where **F** represents the explicit forces appearing in Eq. (6), α is a numerical factor, and S is the semi-implicit operator. Our choice for S is the following

(10) .

S is the sum of the linearized MHD waves and sound waves operators. This choice of S is motivated by the fact that the Alfvén time scale determines the stiffness of the problem in the lower corona. However S is easier to invert than the full MHD operator. The expression for S minimizes the following functional

(11) $$I(\mathbf{v}) = \frac{1}{2}\int_V \left[\left|\nabla\times(\mathbf{v}\times\mathbf{B})\right|^2 + \gamma p(\nabla\cdot\mathbf{v})^2 + 2\mathbf{S}\cdot\mathbf{v}\right]dV .$$

We have made sure that the numerical discretization of S preserves the self-adjointess of the analytical operator. The operator is inverted using the same parallel, preconditioned

CG solver implemented to invert the resistive diffusion operator in the induction equation.

4. VALIDATION OF THE NEW FEATURES IMPLEMENTED IN THE CODE

4.1 The Sod's Problem

We have conducted another test of the implementation of the hydrodynamic equations in MH4D by reproducing the Sod's problem (Sod, G. A. 1978, J. Comp. Phys., 27, 1). This consists of the following: at t=0 a diaphgram separates a tube in two regions filled with a fluid with different densities and pressures.

(12) , .

The specific heat ratios _ is set to 1.4. At t>0 the diaphgram is broken. We have designed a cylindrically shaped grid of radius 0.5 and height 1 with 10300 vertices and 50525 cells. We have evolved the hydrodynamic equations in MH4D stopping before any wave has reached the left or right boundary. The results of the simulation are graphically presented in Fig. 1 (velocity), 2 (pressure), and 3 (density). A shock wave propagates to the right, a rarefaction wave to the left, and a contact discontinuity, visible in the density plot (Fig. 3), follows the shock.

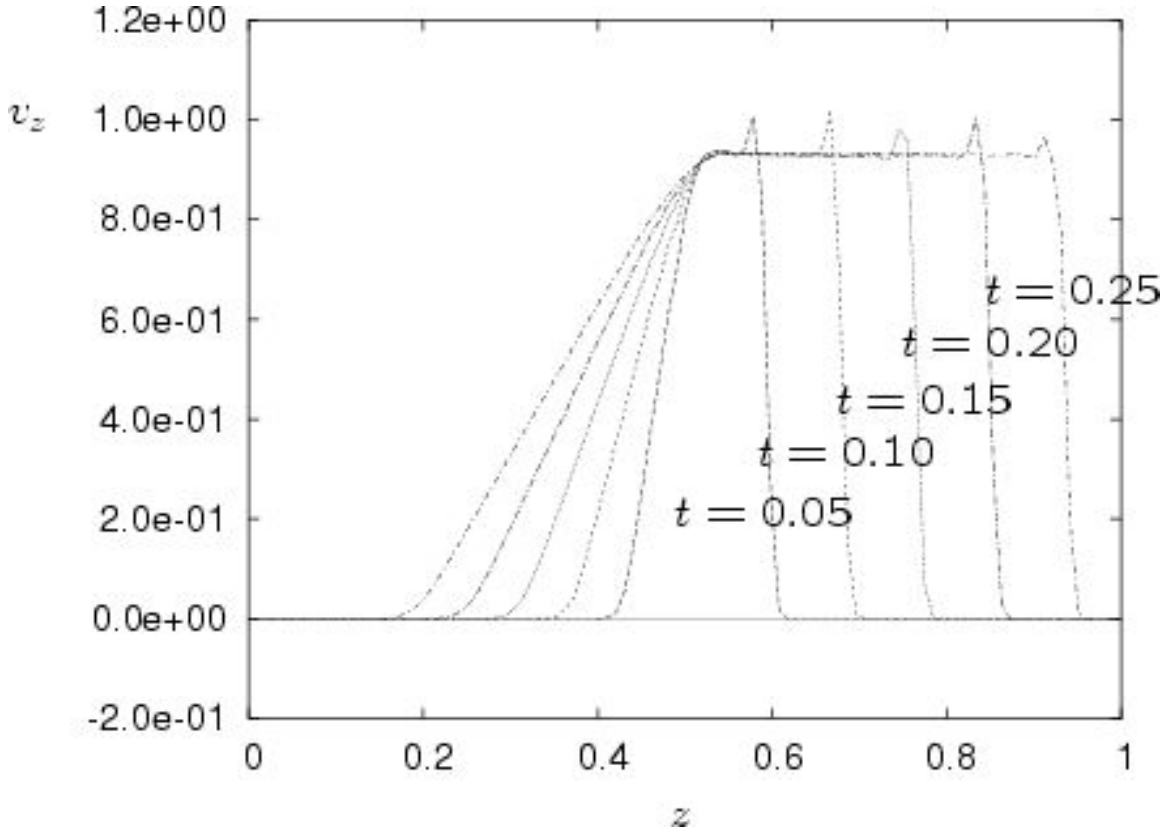

FIG. 1. The component of the velocity along the tube in the Sod's problem at different instants in time. After the diaphgram is broken a shockwave propagates from the left to the right.

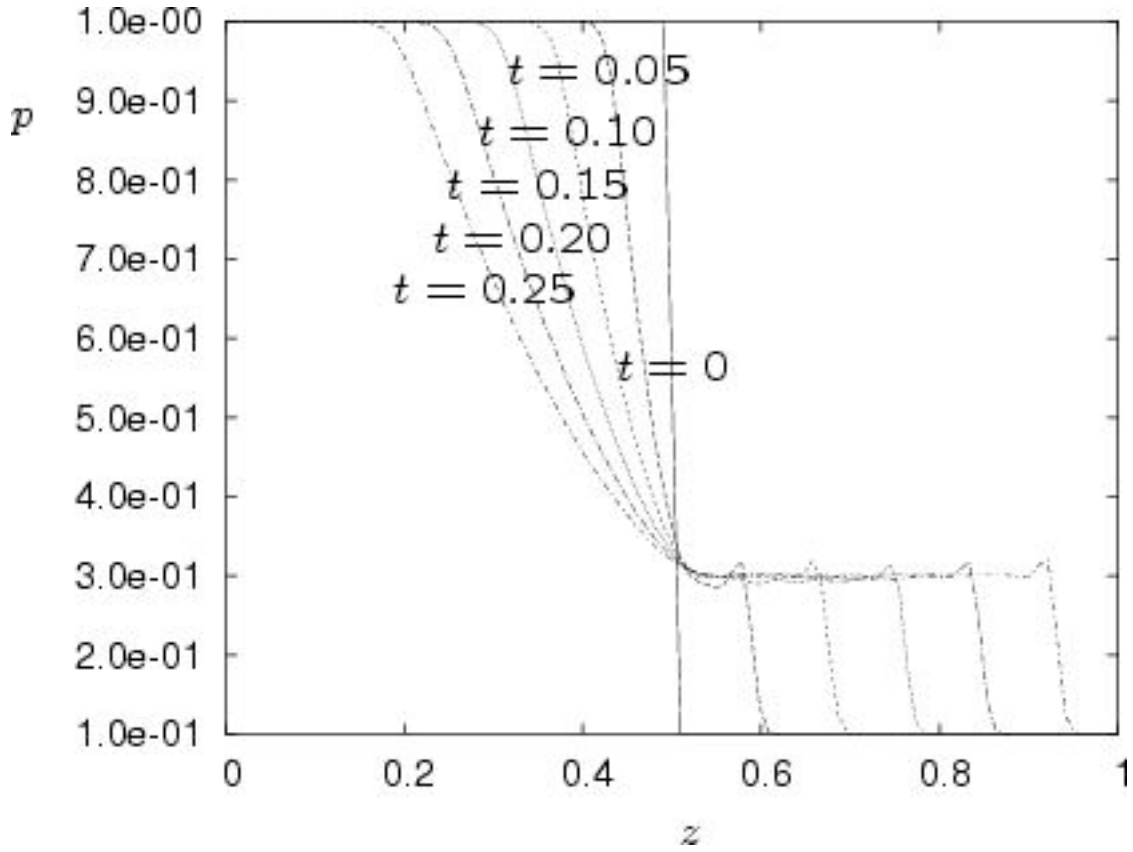

FIG. 2. Evolution of the pressure in the Sod's problem. A shock wave moves rightward and a rarefaction wave leftward.

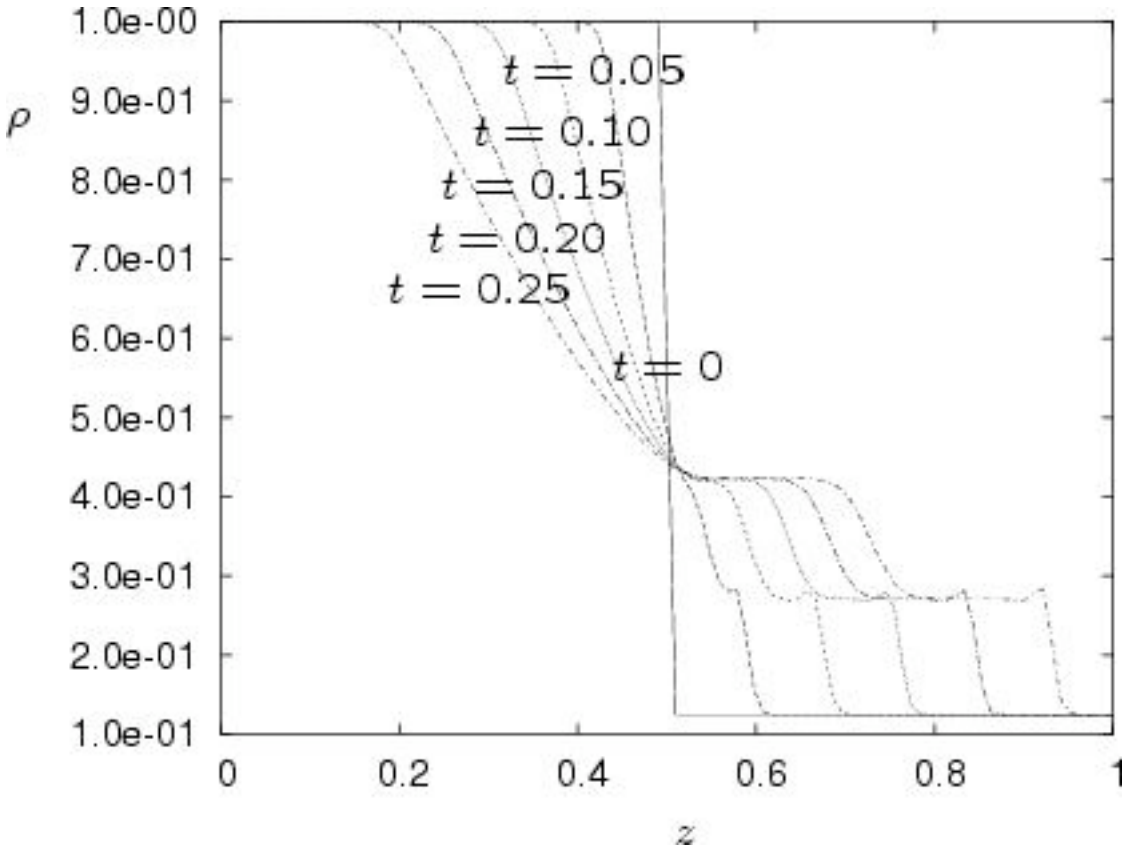

FIG. 3. Evolution of the density in the Sod's problem. We notice a shock wave propagating to the right followed by a contact discontinuity. A rarefaction wave moves to towards the left.

4.2 Alfvén Waves in a Cylinder

We have tested the implementation of the MHD equations by reproducing eigenfunctions of the linearized equations (i.e. Alfvén waves). The equations for linear Alfvén waves are:

(13) —— ,

(14) —— .

We have used δ to indicate the perturbed quantities. A solution (eigenvector) in a cylinder where $\mathbf{B} = B\hat{\mathbf{z}}$ is

(15) ,

with angular speed

(16) $\sqrt{\quad}$.

is an arbitrary function of r. Equation (14) represents a torsional Alfvén wave.

For $k = \pi$, $\rho = 1$, $B = 1$, the theoretical period is $T = 2$. For a cylindrical computational domain of radius and height equal to one, we have designed a grid of 420 vertices and 1692 cells. We have applied the perturbation as in Eq. (15) and advanced Eqs. (1-6) with MH4D using both the explicit and the semi-implicit time advancement with no noticeable difference between the two. In Fig. 4 we show the time history of the kinetic energy, which shows a period of 1, as expected. In Figs. 5 and 6 we show respectively the poloidal component of the magnetic field at four instants in time.

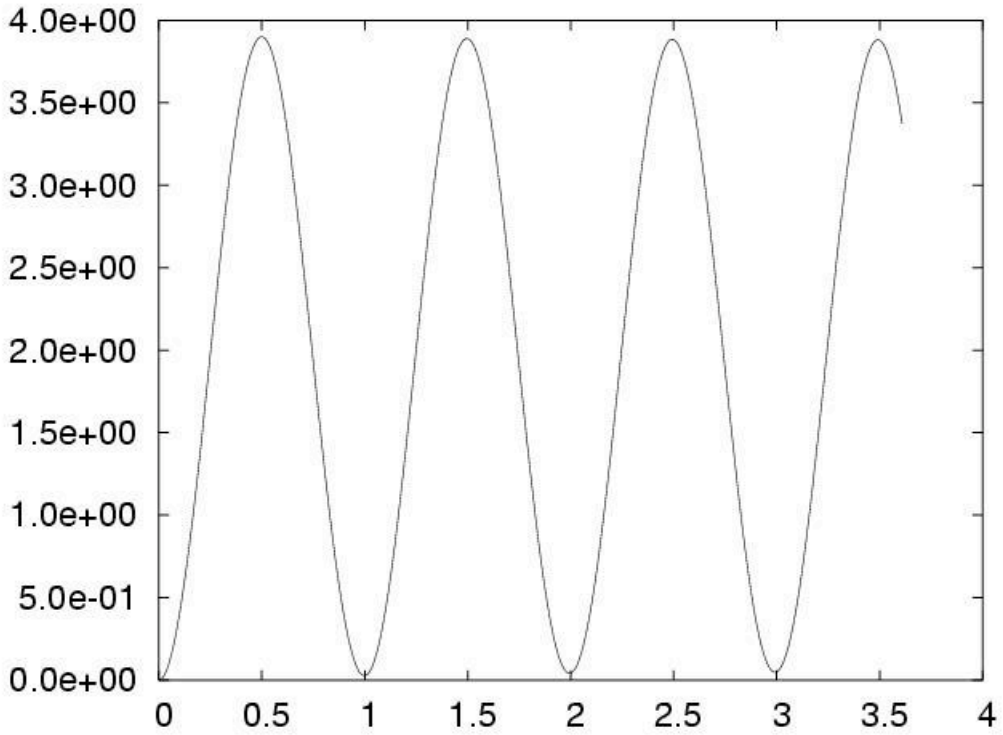

FIG. 4. Kinetic energy as a function of time for the case of the torsional Alfvén wave eigenmode. in a cylinder.

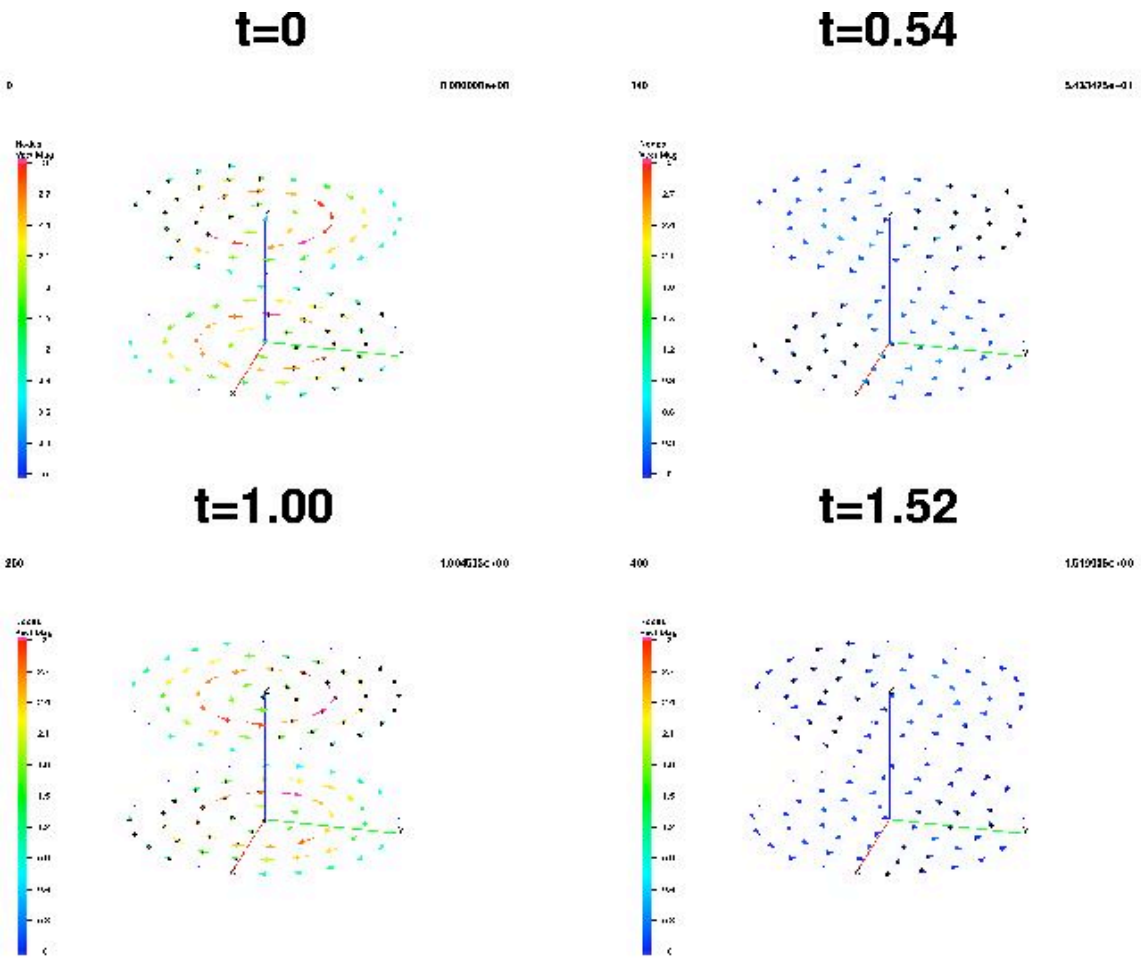

FIG. 5. The poloidal magnetic field is shown at four instants in time in the simulation of a torsional Alfvén wave in a cylinder obtained with MH4D. The vectors are colored according to their magnitude.

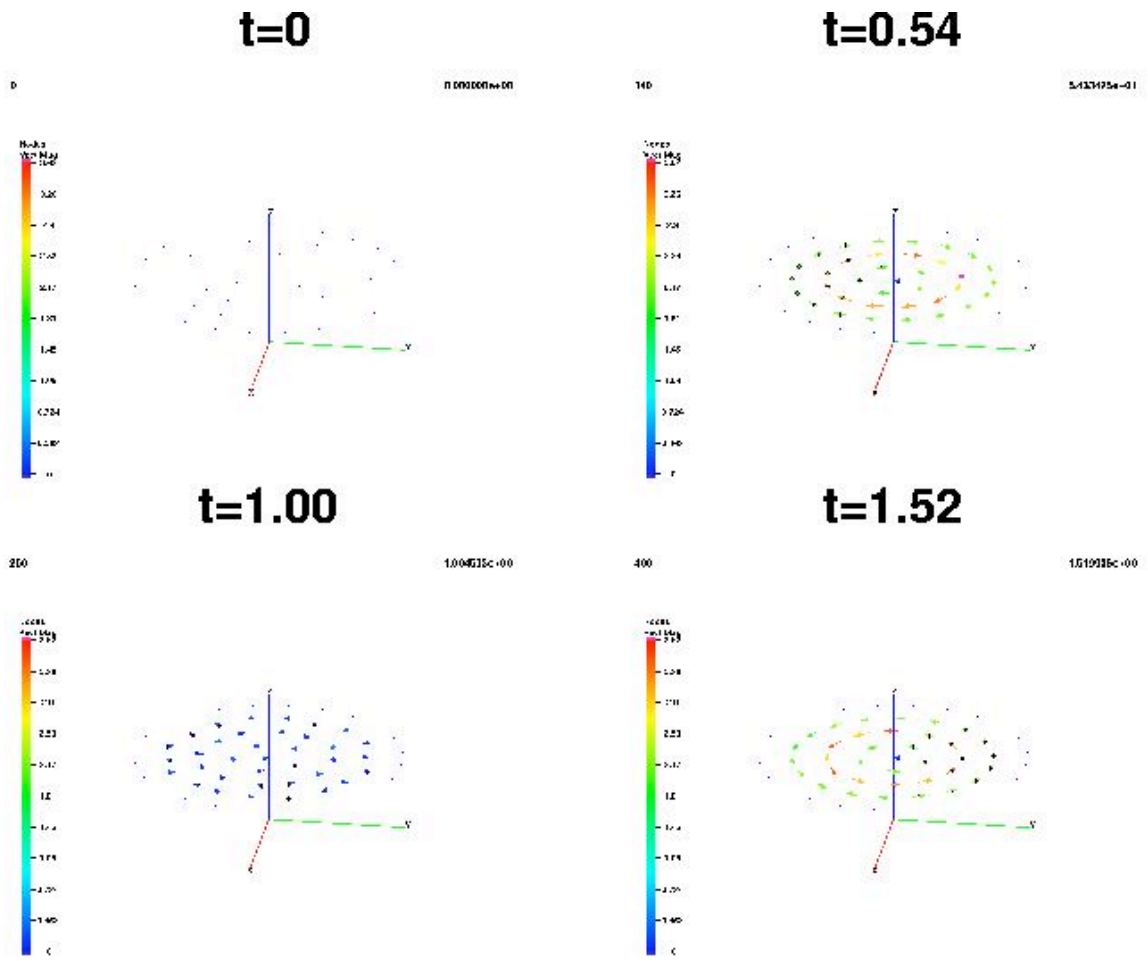

FIG. 6. The poloidal velocity field is shown at four instants in time in the simulation of a torsional Alfvén wave in a cylinder obtained with MH4D. The vectors are colored according to their magnitude.

MH4D Progress Report

3rd and 4th Quarters FY04

June 7, 2003 – December 31, 2003

We report progress for the development of MH4D for the third and fourth quarters of FY2004, June 7, 2003 – December 31, 2003.. In this report we describe progress in the following areas

Presentation of a Poster at the AGU Fall Meeting in San Francisco, California, December 8-12, 2003.

Validation of the New Features Implemented in the Code

The nonlinear kink mode in the unstable Gold-Hoyle equilibrium.

Details are given in the following sections.

1. PRESENTATION OF A POSTER AT THE 2003 AGU FALL MEETING

We have attended the American Geophysical Union Fall Meeting that was held in San Francisco, California, between 8 and 12 December 2003. A poster illustrating the structure of the code and the most recent result was presented. (Dalton D. Schnack and Roberto Lionello ``MH4D: an Algorithm for MHD on a Tetrahedral Grid'', *EOS Trans. AGU, 84(46)* Fall Meet. Suppl, Abstract SH21B-0124, 2003). The text of the abstract follows:

> MH4D (Magnetohydrodynamics on a TETRAhedral Domain) is a massively-parallel, device-independent numerical code for the solution of the resistive and viscous MHD equations on an unstructured grid of tetrahedra. The unstructured grid allows the computational domain to be of arbitrary shape and the resolution to be increased in the regions of physical interest. Consequently, a wide range of spatial scales can be studied at the same time, for example active regions can be embedded in the large scale corona. A variational formulation of the differential operators ensures accuracy and the preservation of the analytical properties of the operators ($\nabla \cdot \mathbf{B} = 0$), and self-adjointness of the resistive and viscous operators. The combined semi-implicit treatment of the waves and implicit formulation of the diffusive operators can accommodate the wide range of time scales present in the solar corona. The capability of mesh refinement and coarsening is also included. We have recently implemented the MHD operators and the semi-implicit solve in the momentum equation and will present preliminary results.

2. VALIDATION OF THE NEW FEATURES IMPLEMENTED IN THE CODE

2.1 The nonlinear kink mode in the unstable Gold-Hoyle equilibrium

We write the Gold-Hoyle magnetic equilibrium with nondimensional variables as follows:

(1) $$B_\phi = \frac{r}{1+r^2},$$

(2) $$B_z = \frac{1}{1+r^2},$$

where B_ϕ and B_z are the poloidal and axial components of the magnetic field in cylindrical coordinates and r is the distance from the axis. In a cylinder with height L, the twist is defined as

(3) $$\Phi = \frac{LB_\phi}{rB_z}$$

In the Gold-Hoyle field the twist is constant. When it exceeds a certain threshold value, the equilibrium is unstable to a global kink mode. We decided to reproduce the kink instability in a line-tied configuration, i.e. a case where the magnetic field line are anchored at the top and bottom of the cylinder. Linear theory predicts that an equilibrium with $\Phi=3\pi$ is unstable. Therefore we have built a cylindrical grid with a radius r=20 and with a height $L=3\pi$. The grid is composed of 68441 nodes and 398948 cells and we have portioned the computational domain between sixteen processors (see Fig. 1). The outer radius has been put to 20 in order to minimize the influence of the external wall on the evolution of the kink. The mesh is much finer near the center of the cylinder, where the currents are present. A random perturbation has been applied to the system and the MHD equations have been advanced from t=0 to t=1000 using MH4D. Figure 2 shows the time history of the kinetic energy during the run. After approximately t=400 the kink mode is clearly visible. After t=500 it saturates. Figure 3 has the magnetic energy and shows that the system evolves towards a kinked equilibrium with lower magnetic energy. Figure 4 shows isosurfaces of A_z, the axial component of the magnetic vector potential, at four instants during the evolution of the instability. A_z approximately tracks magnetic field surfaces.

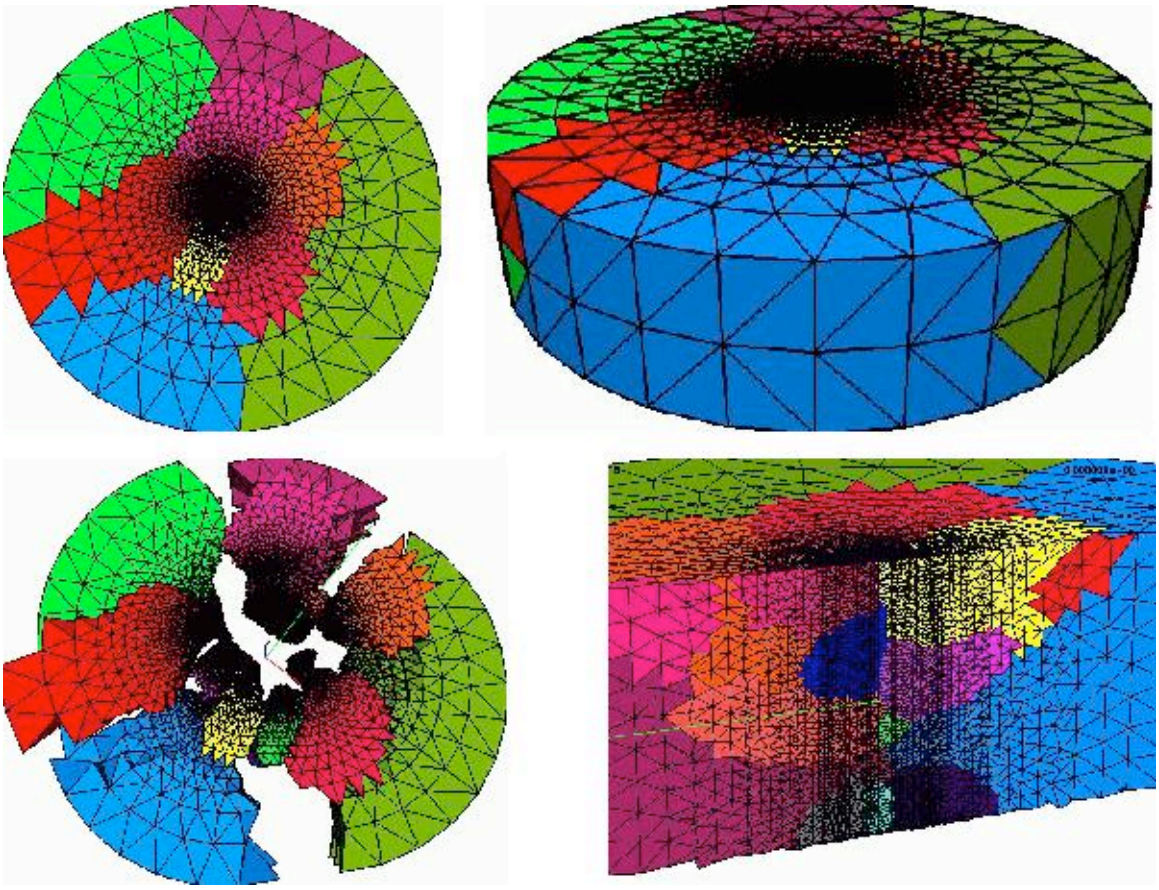

FIG. 1. Four view s of the computational domain in the nonlinear kink simulation. The mesh is divided between sixteen processors and regions belonging to different processors are color coded accordingly.

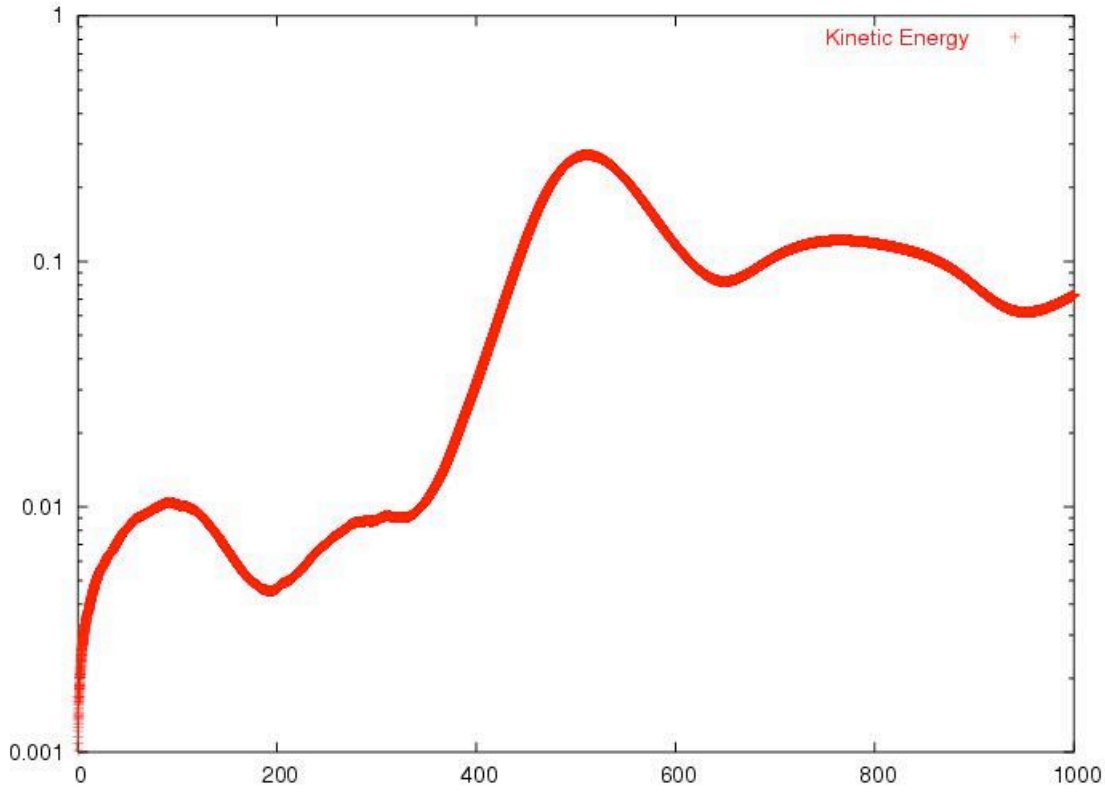

FIG. 2. Evolution of the kinetic energy in the nonlinear kink problem. The kink mode appears on top of a stable mode. After t=500, the system relaxes to a kinked equilibrium.

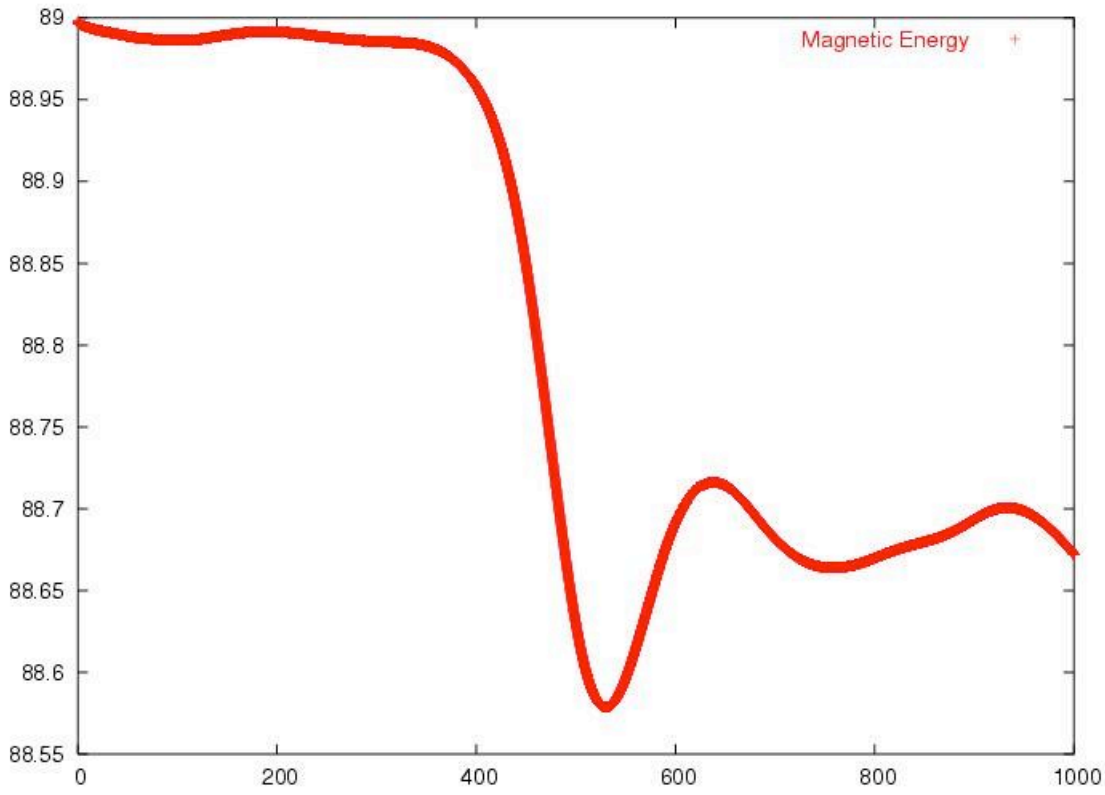

FIG. 3. Evolution of the magentic energy in the nonlinear kink problem. The system evolves toward a kinked equilibrium with lower magnetic energy.

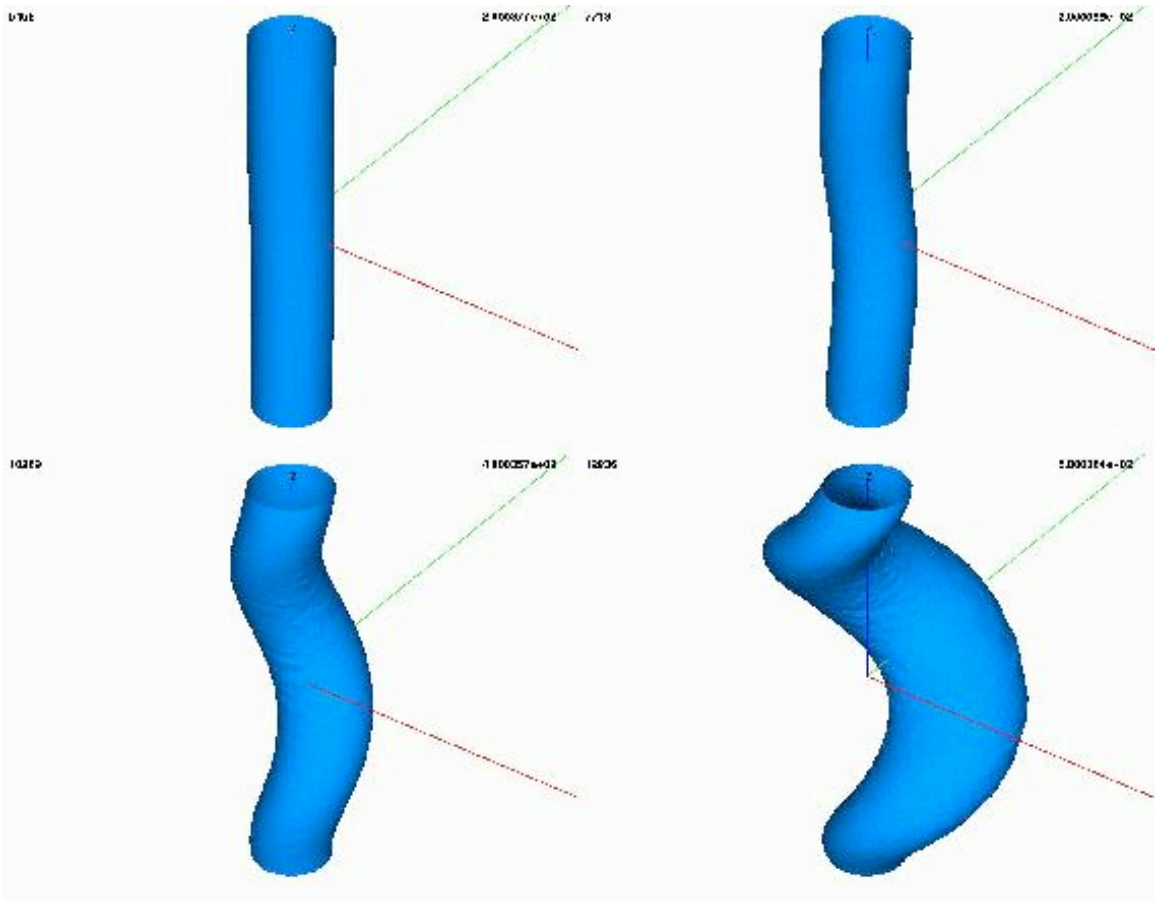

FIG. 4. Isosurfaces of the axial component of the magnetic vector potential A_z. During the evolution of the kink instability at t=200, 300, 400, and 500.

MH4D Progress Report

1st and 2nd Quarters FY05

January 1, 2004 – June 28, 2004

We report progress for the development of MH4D for the first and second quarters of FY2005, January 1, 2004 – June 28, 2004 In this report we describe progress in the following areas:

Presentation of a Poster at the 2004 Joint Assembly (CGU, AGU, SEG, and EEGS) in Montreal, Canada, May 17-21, 2004.

Validation of the New Features Implemented in the Code

The MHD shock problem (Brio, M. and Wu, C. C., J. Comp. Phys. 75, 400 , 1988)

Details are given in the following sections.

1. PRESENTATION OF A POSTER AT THE 2004 JOINT ASSEMBLY.

We have attended the 2004 Joint Assembly, a partnership between CGU, AGU, SEG and EEGS, which was held in Montreal, Canada, between 17 and 21 May 2004. A poster illustrating the structure of the code and the most recent result was presented. (Roberto Lionello and Dalton D. Schnack `` MHD Simulations on an Unstructured Tetrahedral Grid with MH4D '', *EOS Trans. AGU, 85(17,)* Jt. Assem. Suppl., Abstract SH41A-02, 2004). The text of the abstract follows:

> MH4D (Magnetohydrodynamics on a TETRAhedral Domain) is a numerical algorithm to solve the resistive and viscous MHD equations on an unstructured grid of tetrahedra. MH4D is device independent and runs on desktop computers as well as massively-parallel systems. Thanks to the use of an unstructured grid, the computational domain can be of arbitrary shape and the resolution can be increased in the regions of physical interest. Consequently, a wide range of spatial scales can be studied at the same time, for example active regions can be embedded in the large scale corona. A variational formulation of the differential operators ensures accuracy and the preservation of the analytical properties of the operators ($\nabla \cdot \mathbf{B} = 0$), and self-adjointness of the resistive and viscous operators. The combined semi-implicit treatment of the waves and implicit formulation of the diffusive operators can accommodate the wide range of time scales present in the solar corona. The capability of mesh refinement and coarsening is also included. We will present some new results obtained with the full MHD algorithm on the IBM SP3.

2. VALIDATION OF THE NEW FEATURES IMPLEMENTED IN THE CODE

2.1 The MHD shock problem

Brio, M. and Wu, C. C., J. Comp. Phys. 75, 400 , (1988) present the numerical solution of a 1.5 dimensional MHD shock problem. We adapted their problem to cylindrical symmetry, since our code is intrinsically three-dimensional. The grid consists of 482007 nodes and 2717151 cells. It discretizes a computational domain consisting of a cylinder with radius $r = 2$, height $z = 0.05$, with a cylindrical hole extending from $0 \le r < 1$. The grid is partitioned among 16 processors (Fig. 1) . The resolution is enhanced in one sector in order to resolve the small scales without using a prohibitive number of points. As initial conditions we have a diaphgram at $r = 1.5$ separating the fluid into two states, a `left' state (corresponding to $1 \le r < 1.5$):

(1) $$\rho_{left} = 1,\ p_{left} = 1,\ B_r = \frac{1.125}{r},\ B_\varphi = \frac{1.5}{r},$$

and `right' state (corresponding to $1.5 \le r \le 2$):

(2) $$\rho_{right} = 0.125,\ p_{right} = 0.1,\ B_r = \frac{1.125}{r},\ B_\varphi = -\frac{1.5}{r},$$

where ρ is the density, p the pressure, B_r, and B_ϕ and are the radial and poloidal components of the magnetic field in cylindrical coordinate. At t=0 the diaphgram is removed. A rarefaction fan and a slow wave move inwards (leftwards in Brio and Wu, 1988) and a contact discontinuity, a slow shock, and a second rarefaction fan move outwards (rightwards in Brio and Wu, 1988). Figure 2 shows cutlines in the sector with enhanced resolution for the density, pressure, radial and poloidal velocity, and poloidal magnetic field at t=1. It can be compared with Figs. 2-6 in Brio and Wu (1988). A cutplane of the density is shown in Fig. 3.

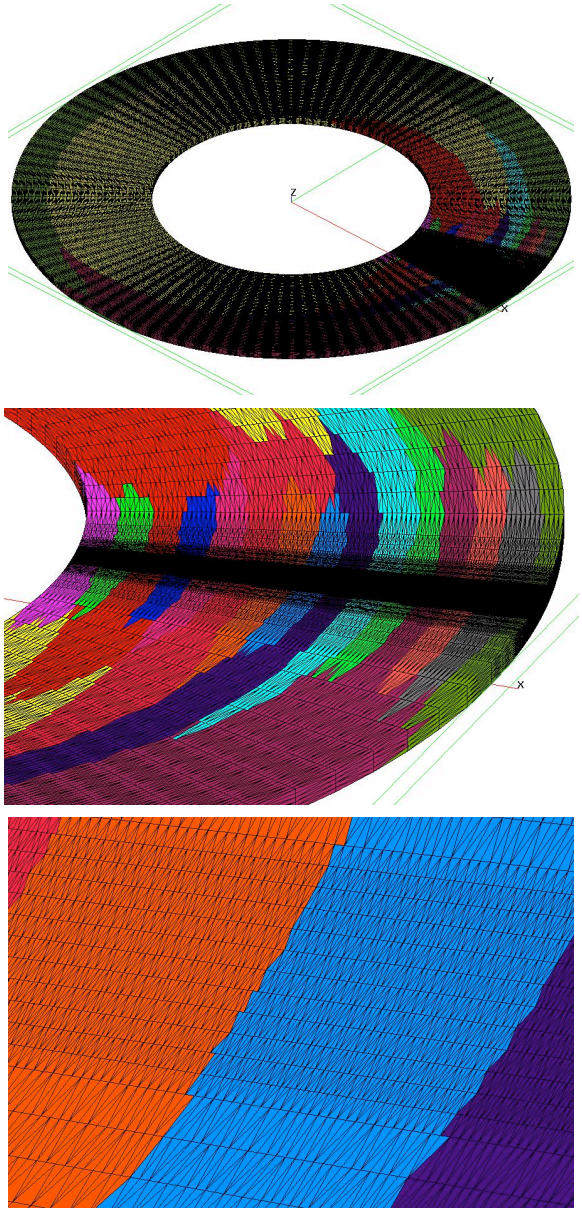

FIG. 1. Three views of the computational domain in the MHD shock simulation. The resolution is enhanced in one sector. The mesh is divided between sixteen processors and regions belonging to different processors are color coded accordingly.

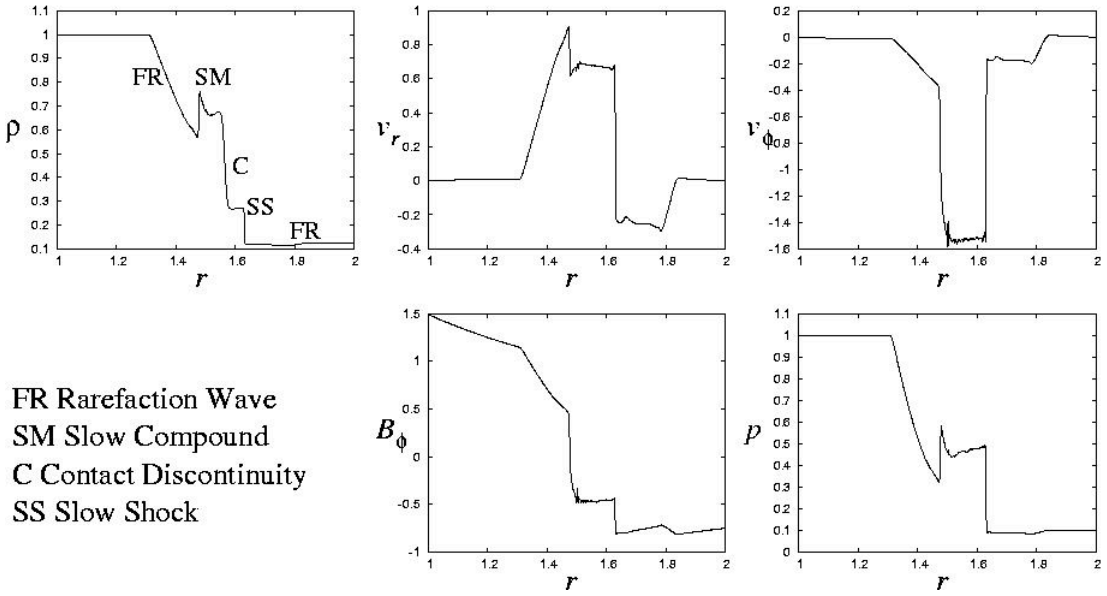

FIG. 2. The density, radial and tangential velocity, the poloidal magnetic field, and the pressure at t=1 in the MHD shock simulation. A rarefaction fan and a slow wave are propagating leftwards, a contact discontinuity, a slow shock, and another rarefaction wave are moving rightwards.

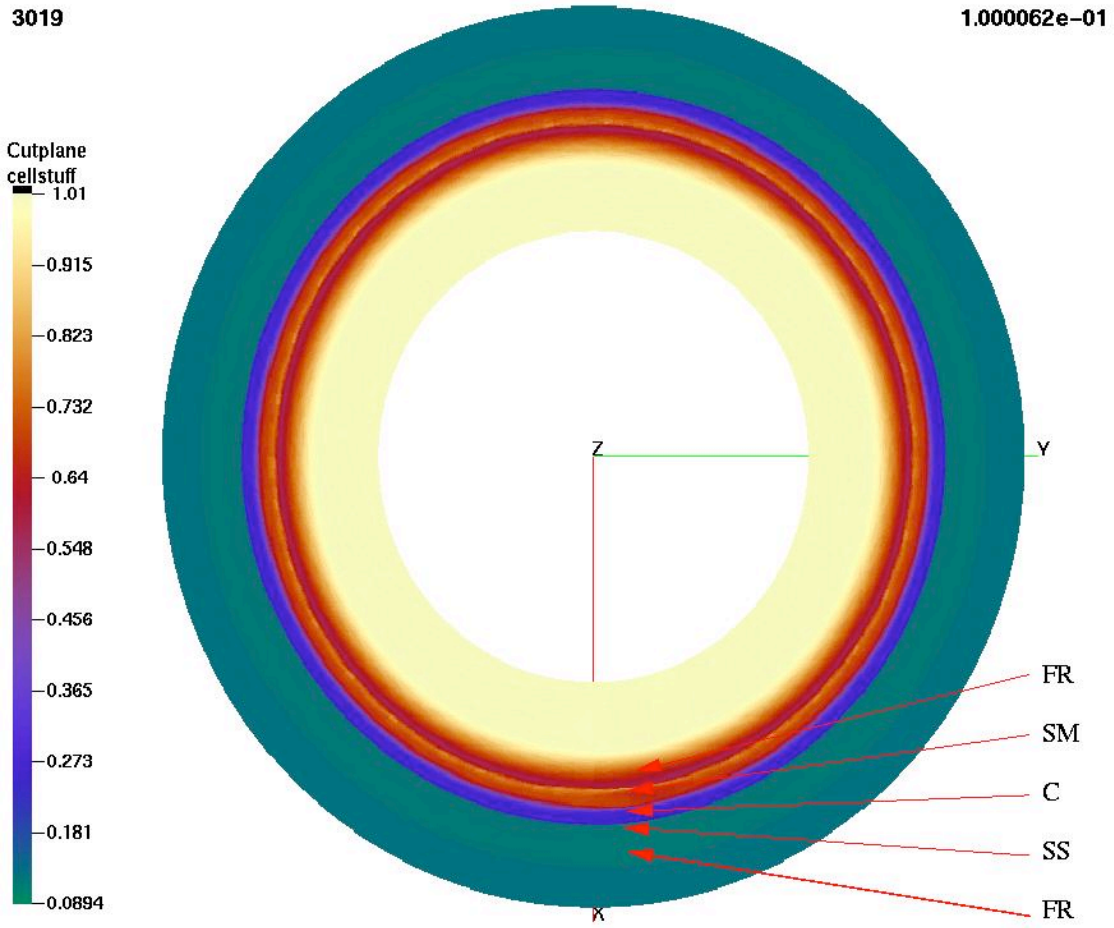

FIG. 3. MHD shock simulation: a cutplane of the density is drawn through the computational domain. See Fig. 2 for the meaning of the symbols.

MH4D Progress Report

3nd and 4th Quarters FY05

June 28, 2004 – January 1, 2005

We report progress for the development of MH4D for the third and fourth quarters of FY2005, June 28, 2004 – January 1, 20045. In this report we describe progress in the following areas:

Presentation of a Poster at the 2004 Fall AGU Meeting to be held in San Francisco, CA, December 13-17, 2004.

Supersonic Solar Wind Problem

Details are given in the following sections.

1. PRESENTATION OF A POSTER AT THE 2004 AGU MEETING.

We have submitted an abstract for the 2004 Fall AGU meeting, which is to be held in San Francisco, CA , between 13 and 17 December 2004. A poster illustrating the structure of the code and the most recent result will be presented. (Dalton D. Schnack and Roberto Lionello `` MHD Modeling of the Solar Wind with with MH4D''). The text of the abstract follows:

> MH4D (Magnetohydrodynamics on a TETRAhedral Domain) is a numerical code to solve the resistive and viscous MHD equations on an unstructured mesh of tetrahedra. MH4D is device independent and runs on desktop computers as well as massively-parallel systems. Thanks to the use of an unstructured grid, the computational domain can be of arbitrary shape and the resolution canbe increased in the regions of physical interest. Consequently, a wide range of spatial scales can be studied at the same time, for example active regions can be embedded in the large scale corona. A variational formulation of the differential operators ensures accuracy and the preservation of the analytical properties of the operators ($\nabla \cdot \mathbf{B} = 0$),and self-adjointness of the resistive and viscous operators. The combined semi-implicit treatment of the waves and implicit formulation of the diffusive operators can accommodate the wide range of time scales present in the solar corona. The capability of mesh refinement and coarsening is also included. We will present a model of the solar wind obtained with the full MHD algorithm on the IBM SP3.

2. SUPERSONIC SOLAR WIND PROBLEM

We simulated the supersonic solar wind starting from a distance of 30 solar radii from the center of the Sun up to 1 AU. We created a nonuniform mesh of 58,488 nodes and 355,5609 cells. The resolution is approximately 8.6 degrees everywhere except in a cone centered around the x axis where the resolution is 2.1 degrees. A plot of the mesh is presented in Fig. 1. On the inner surface we specify the following quantities:

(1) ρ_s = 2.44E-05 ρ_0, p_s= 1.84E-06 p_0, $B_r|_s = 1.11\text{E}-03\,\text{sign(latitude)}B_0$

where ρ_s = 1.E –08 cm^{-3}, $p_0 = 0.387$ dyne/cm^2, and B_0 = 2.205 G, which are our reference values for the solar corona. The initial condition is a Parker solar wind flow with the ratio of specific heats $\gamma = 1.05$. We advance the MHD equations in time for 400 t_0, which translates to 6.7 days, until steady state is reached. In Fig. 2 we show plane cuts of the density and of the pressure in a base 10 logarithmic scale.

Figure 3 shows the mesh superimposed with some velocity vectors. The mesh and the velocity vectors are colored according to the magnitude of the velocity. The solution is somewhat noisy in the region with coarse resolution, but less so in the sector with high resolution. In Fig. 4 we show the region of where the magnetic field is zero (current sheet) plus a cut sphere colored according to the radial component of *B* at 30 solar radii. In this figure it is also evident how the improved resolution in the cone around the x axis makes for a less noisy solution than in the region around it.

It is clear from these figures that the solutions are unacceptably noisy. We have not clearly identified the source of these errors, but it appears to be associated with the local detailed geometry of the grid. We are presently re-writing parts of the code to define the momentum density at the centroids of tetrahedra, instead of at the vertices. This will put the momentum density on the same footing as the mass density and pressure, and hopefully will lead to smoother solutions.

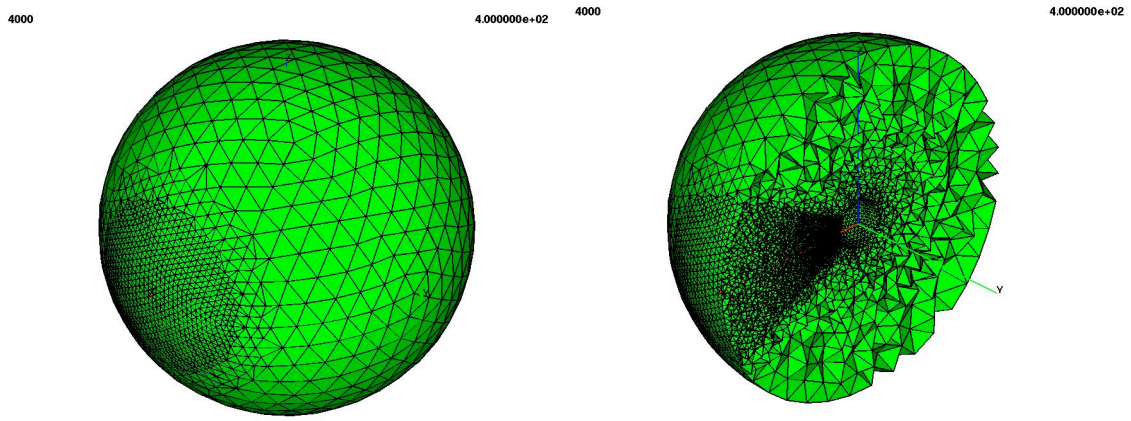

FIG. 1. Two views of the computational domain in the MHD supersonic solar wind simulation. The domain extends from 30 to 215 solar radii (215 solar radii= 1AU). The resolution is enhanced in a cone centered around the x axis.

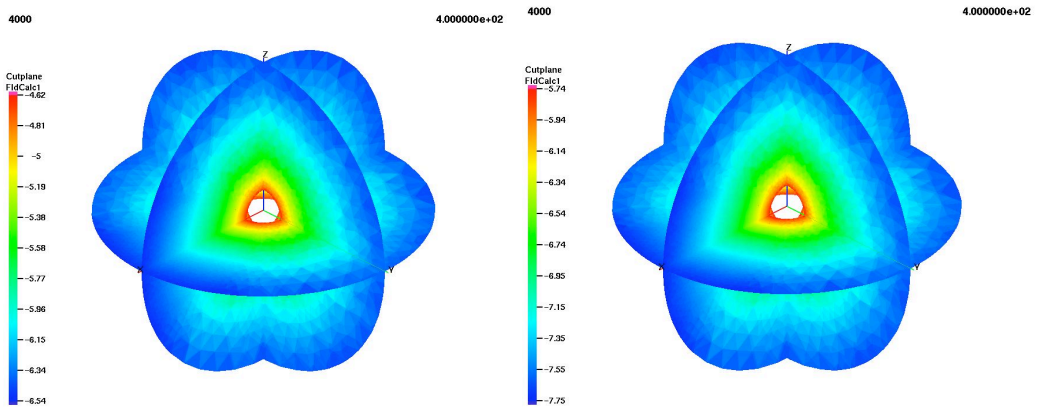

FIG. 2. Plane cuts of the density (left) and of the pressure (right) in a base 10 logarithmic scale .

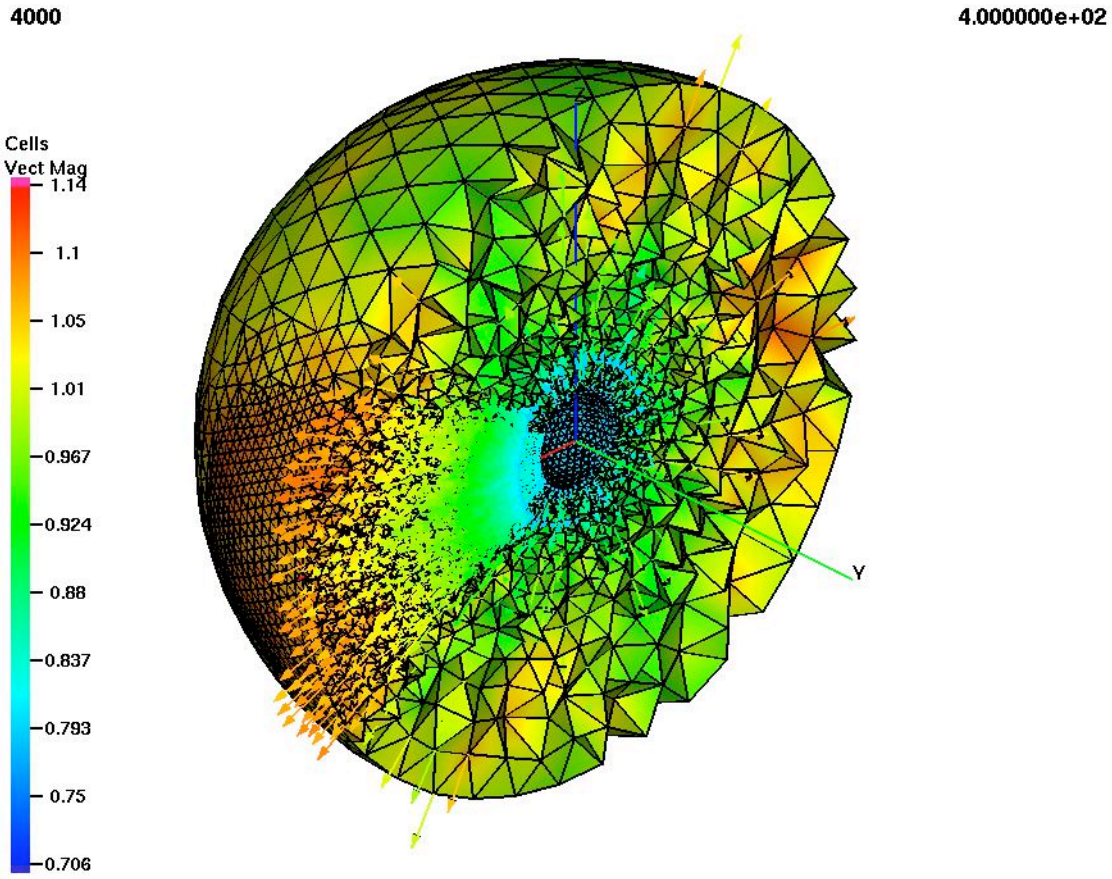

FIG. 3. The velocity vectors superimposed to a mesh cut. The cells and the arrows are colored according to the magnitude of the velocity. Notice how the solution is better in the region where the resolution is higher.

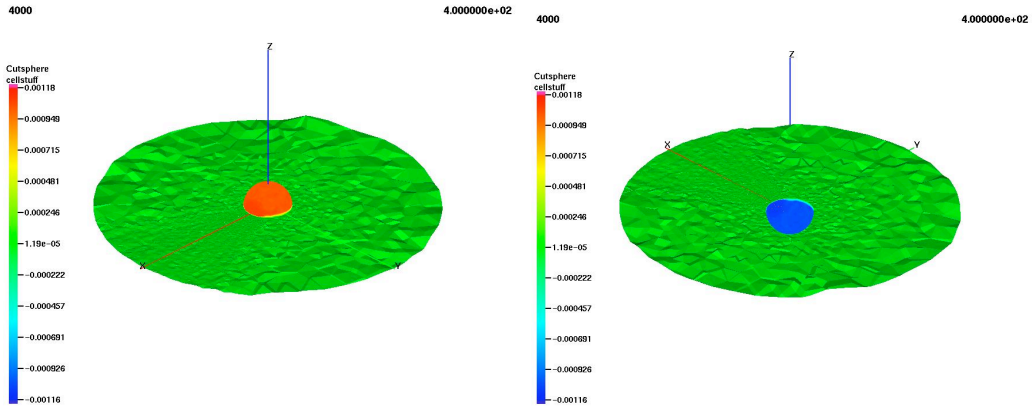

FIG. 4 Two views of the regions where the radial magnetic field is zero, corresponding to the current sheet, plus a cut sphere of the magnitude of the magnetic field at 30 solar radii.

MH4D Progress Report

1st and 2nd Quarters FY06

January 2, 2005 – June 28, 2005

We report progress for the development of MH4D for the first and second quarters of FY2006, January 2, 2005 -- June 28, 2005. In this report we describe progress in the following areas:

Oral Presentation at the 2005 AISRP PI Meeting that was held at the NASA Ames Research Center, on April 4-6, 2005..

Presentation of a Poster at the 2005 Joint Assembly that was held in New Orleans, LA, on May 23-27, 2005.

Development of a cell-centered advection scheme for the momentum equation.

Propagation of a disturbance in the supersonic solar wind.

Details are given in the following sections.

1. ORAL PRESENTATION AT THE 2005 AISRP PI MEETING

We participated to the 2005 AISRP PI Meeting, which was held at the NASA Ames Research Center CA , between 4 and 6 April 2005. The text of the abstract of the oral presentation follows:

Highlights: MH4D is a platform-independent, semi-implicit algorithm to solve the viscous and -resistive MHD equations on an unstructured tetrahedral grid. During the past year we have completed the implementation of the full, semi-implicit MHD equations into MH4D. We have tested the code on well-known problems, such as the Brio and Wu MHD shock and the supersonic solar wind.

Relevance to NASA: Thanks to the use of unstructured grids, the field of application of MH4D is very large. Domain of arbitrary shape and with non-uniform resolution can be modeled. Therefore the code can be applied to different fields that are relevant to NASA, such as solar physics, space physics, planetary physics, astrophysics, etc.

Application to NASA Mission and Programs: Although our code is still in a development phase, our colleague Dr. Pete Riley has started to use MH4D for his heliospheric investigation supported from NASA SEG-GI and SR&T contracts.

Tracking: Once the code is ready to be released to the general user, we plan to ask the users to register before downloading the code from our web site.

Upcoming Plans: In the upcoming year we intend to complete the testing phase and release an alpha version of the code to selected users.

3. DEVELOPMENTOF A CELL-CENTERED ADVECTION SCHEME FOR THE MOMENTUM EQUATION

Simulations of the supersonic solar wind have convinced us that the vertex-centered advection algorithm in the momentum equation does not perform adequately when used in expanding grids. In the past simulations (e.g. the Brio-Wu MHD shock problem) this problem did not appear because the cell volume in the region of physical interests was fairly constant. The control volume around vertices is a not a tetrahedron but a complicated solid figure that does not enjoy the same geometrical properties. Therefore we wrote a new advection scheme for cell-centered vector quantities to be used in the momentum equation. In Fig. 1 we compare the results for a simple test case consisting of a cold fluid expanding from 30 solar radii to 1 AU. The analytical solution gives a velocity with constant radial component. The result obtained with the vertex-centered scheme is clearly not acceptable. The cell-centered algorithm yields a result with an error below 1%. Since we have found that similar problems occur in the induction equation., which advances the vertex-centered vector potential, we have now decided to advance the cell-centered magnetic field directly and we are currently coding and testing new routines to implement that feature.

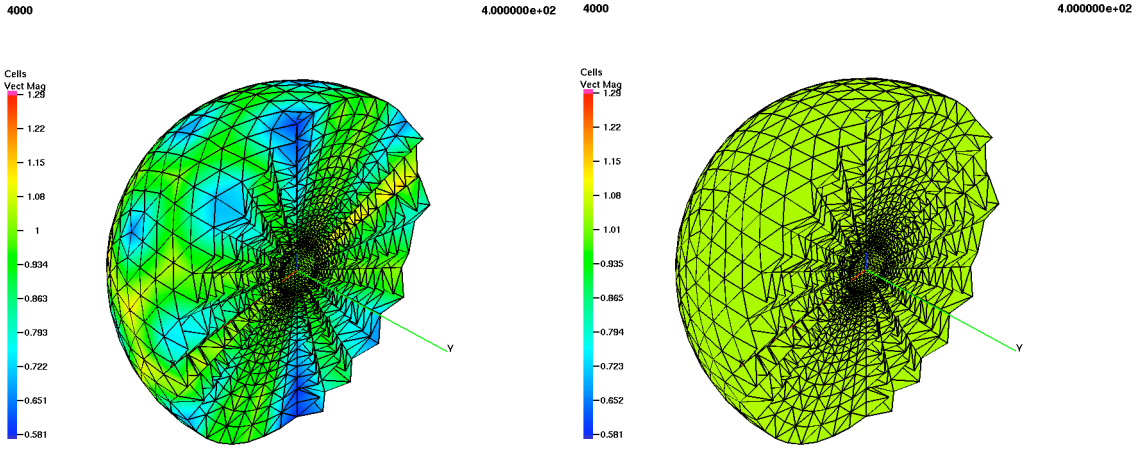

FIG. 1. Test of the advection algorithm with momentum on vertices (left) and on centroids (right). The color scale represents the magnitude of the velocity, which is supposed to be constant in the radial component. While the first algorithm is clearly not acceptable, the second gives a result with an error below 1%.

4. PROPAGATION OF A DISTURBANCE IN THE SUPERSONIC SOLAR WIND.

We simulated the propagation of a disturbance (pressure pulse) in supersonic solar wind starting from a distance of 30 solar radii from the center of the Sun up to 5 AU. We created a spherically symmetric mesh of 148,596 nodes and 875,520 cells. The resolution is approximately 4.5 degrees everywhere. On the inner surface we specify density, pressure, and velocity around an axis of symmetry inclined 20 degrees from the rotation axis (see Fig.2). The slow wind is confined in a 15 degree wide belt that is surrounded by the fast wind. The whole pattern rotates according with the solar rotation rate.

We advance the hydrodynamics equations in time for 30 days until steady state is reached. At that point a disturbance is injected into the domain with the following velocity and density:

$$v = v_{\text{cme}} = v_{\text{fast}}, \qquad \rho = \rho_{\text{cme}} = 4 \times \rho_{\text{slow}}. \tag{1}$$

The pulse is injected along the *y*-axis by modifying the boundary conditions in a cone with angular size controlled by

$$\theta = \theta_{\text{cme}} \sin\left(\frac{\pi(t - t_0)}{\tau_{\text{cme}}}\right), \tag{2}$$

where θ_{cme} is 40 degrees, t_0 is the instant when the disturbance starts, and τ_{cme} is the duration of the disturbance (12 hours). Figure 3 shows cutplanes in the ecliptic plane of the density scaled with r^2 as the pulse propagates through the heliosphere. The disturbance interacts with the double spiral structure formed by the slow (denser) solar wind and the fast solar wind.

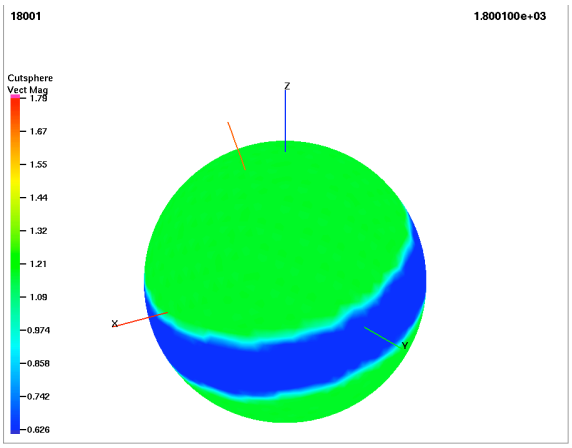

Fast Wind:
$v_r = 560$ km/s
$T = 1.85 \times 10^6$K
$\rho = 152$ cm^{-3}
Slow Wind:
$v_r = 300$ km/s
$T = 3.45 \times 10^6$K
$\rho = 529$ cm^{-3}

FIG. 2. Boundary conditions at 30 solar radii: a 15 degree belt of slow wind, surrounded by fast wind, lies around an axis of symmetry inclined 20 degrees with respect of the rotation axis. The whole pattern rotates around the rotation axis once every 27 days.

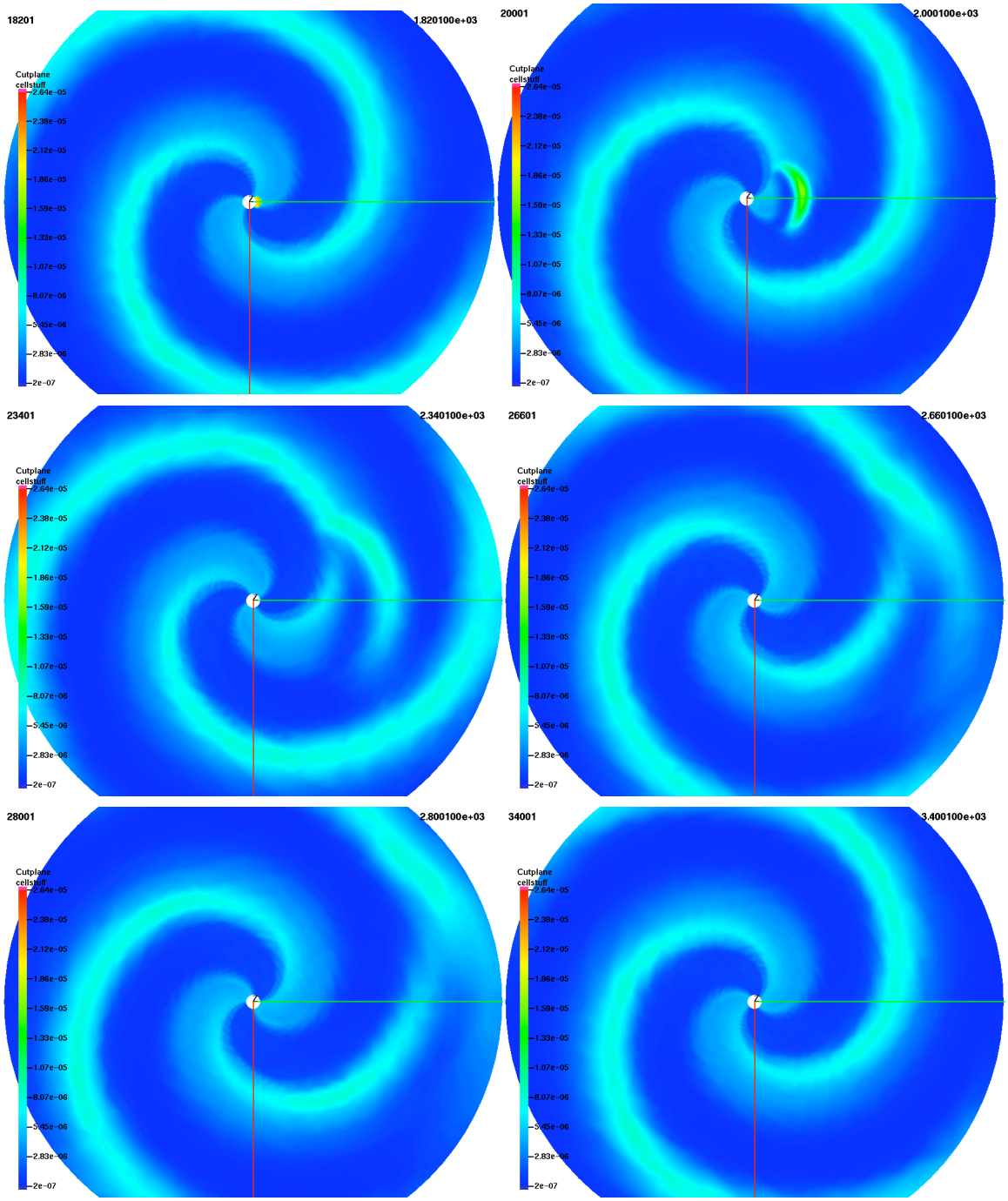

FIG. 3. Propagation of a disturbance in the supersonic solar wind from 30 solar radii to 5 AU at 6 instants in time. The plots show cuts in the ecliptic plane of the density scaled with r^2. The denser slow solar wind and the fast solar wind streams form a double spiral structure through which the pulse propagates.